



# CHORUS

This is the accepted manuscript made available via CHORUS. The article has been published as:

## Quantum interference in laser-induced nonsequential double ionization

Wei Quan, XiaoLei Hao, YanLan Wang, YongJu Chen, ShaoGang Yu, SongPo Xu, ZhiLei Xiao, RenPing Sun, XuanYang Lai, ShiLin Hu, MingQing Liu, Zheng Shu, XiaoDong Wang, WeiDong Li, Wilhelm Becker, XiaoJun Liu, and Jing Chen

Phys. Rev. A **96**, 032511 — Published 29 September 2017

DOI: [10.1103/PhysRevA.96.032511](https://doi.org/10.1103/PhysRevA.96.032511)

# Quantum interference in laser-induced nonsequential double ionization

Wei Quan<sup>1</sup>, XiaoLei Hao<sup>2\*</sup>, YanLan Wang<sup>1,3</sup>, YongJu Chen<sup>1,3</sup>, ShaoGang Yu<sup>1,3</sup>, SongPo Xu<sup>1,3</sup>, ZhiLei Xiao<sup>1,3</sup>, RenPing Sun<sup>1,3</sup>, XuanYang Lai<sup>1</sup>, ShiLin Hu<sup>4,5</sup>, MingQing Liu<sup>5</sup>, Zheng Shu<sup>5</sup>, XiaoDong Wang<sup>6</sup>, WeiDong Li<sup>2</sup>, Wilhelm Becker<sup>7,8</sup>, XiaoJun Liu<sup>1†</sup> & Jing Chen<sup>4,5‡</sup>

<sup>1</sup> *State Key Laboratory of Magnetic Resonance and Atomic and Molecular Physics and Center for Cold Atom Physics, Wuhan Institute of Physics and Mathematics, Chinese Academy of Sciences, Wuhan 430071, China.*

<sup>2</sup> *Institute of Theoretical Physics and Department of Physics, Shanxi University, 030006 Taiyuan, China.*

<sup>3</sup> *School of Physics, University of Chinese Academy of Sciences, Beijing 100080, China.*

<sup>4</sup> *HEDPS, Center for Applied Physics and Technology, Beijing 100084, China.*

<sup>5</sup> *Institute of Applied Physics and Computational Mathematics, P. O. Box 8009, Beijing 100088, China.*

<sup>6</sup> *College of Physics and Electronic Engineering,*

*Northwest Normal University, Lanzhou, 730070, China.*

<sup>7</sup> *Max-Born-Institut, Max-Born-Strasse 2a, 12489 Berlin, Germany.*

<sup>8</sup> *National Research Nuclear University MEPhI, Kashirskoe Shosse 31, 115409 Moscow, Russia.*

(Dated: August 31, 2017)

Quantum interference plays an important role in various intense-laser-driven atomic phenomena, e.g., above-threshold ionization and high-order harmonic generation, and provides a useful tool in ultrafast imaging of atomic and molecular structure and dynamics. However, it has eluded observation in nonsequential double ionization (NSDI), which serves as an ideal prototype to study electron-electron correlation. Thus far, NSDI usually could be well understood from a semiclassical perspective, where all quantum aspects have been ignored after the first electron is tunneled. Here we perform coincidence measurements for NSDI of xenon subject to laser pulses at 2400 nm. It is found that the intensity dependence of the asymmetry parameter between the yields in the 2nd and 4th quadrants and those in the 1st and 3rd quadrants of the electron-momentum-correlation distributions exhibits a peculiar fast oscillatory structure, which is beyond the scope of the semiclassical picture. Our theoretical analysis indicates that this oscillation can be attributed to interference between the contributions of different excited states in the RESI channel (recollision-excitation with subsequent ionization). Our work demonstrates the significant role of quantum interference in NSDI and may create a new pathway towards manipulation and imaging of the ultrafast atomic and molecular dynamics in intense laser fields.

PACS numbers: 32.80.-t, 32.80.Fb, 42.50.Hz

## I. INTRODUCTION

Quantum mechanics implies via wave-particle duality wavelike phenomena for massive particles so that interference is an, in principle, omnipresent effect. Especially, in strong-field atomic and molecular physics, where the presence of the field makes available different paths into the same final state [1], interference should be ubiquitous. Indeed, great efforts have been made to explore the important role of interference in atomic and molecular above-threshold ionization (ATI) [2–13] and high-order harmonic generation (HHG) [14–18]. In fact, the ATI peaks in the photoelectron spectrum can be understood as an intercycle interference effect [19] and interference fringes in the photoelectron momentum distribution (PMD) are attributed to intracycle interference, which can be interpreted as a hologram that encodes the structure and the dynamics of the atoms and molecules with attosecond temporal and angstrom spatial resolu-

tion [20–23]. In molecular HHG, interference between the photoelectron wavepackets generated from the different nuclear centers will modify the HHG spectrum [14–18] and, based on this, HHG spectroscopy has been extensively employed in ultrafast imaging of molecular structure and dynamics [24–27].

However, in stark contrast to the well established quantum interference features in ATI and HHG and their increasing applications in ultrafast science, no solid evidence of interference has been identified for another important strong-field process, i.e., nonsequential double ionization (NSDI) [28, 29], even though it has attracted much attention for the last decades because it involves electron-electron correlation [28–31]. It is still an open question if and how interference effects will play a significant role in the observable NSDI dynamics. At first glance, this may be surprising considering the fact that electron rescattering [32, 33], which is responsible for the above-mentioned ATI and HHG processes, has also been established as the main mechanism underlying NSDI. However, compared with ATI and HHG, for which electron correlation plays a negligible role if any, the interaction between electrons may bring much more complexity to the NSDI process and, more importantly, may obscure the possible interference pattern in the measured

†xjliu@wipm.ac.cn

‡chen\_jing@iapcm.ac.cn

\*xlhao@sxu.edu.cn

PMD. In addition to its principal significance as an inherent quantum feature, quantum interference in NSDI, similarly as in ATI and HHG, may also find potential applications in ultrafast science, in particular for ultrafast imaging of many-electron dynamics, for which electron correlation plays an indispensable role.

According to the electron rescattering picture, as a first step of NSDI, a bound electron tunnels through the potential barrier formed by the intense laser field and the atomic potential. The freed electron may then be driven back to collide with the parent ionic core. If its return energy is high enough, the electron will knock out the second electron from the core to induce double ionization (DI) via recollision-impact-ionization (RII). In this pathway, the second electron is directly pumped into a continuum state. The subsequent motion of both electrons can be described by the classical Newtonian equations. Interference arising from the quantum aspects of the electron wavepackets so far has not been observed. Indeed, many of the key experimental features related to this pathway can be well reproduced by such classical models (for reviews, see e.g., Ref. [31]). Moreover, the unavoidable complexities of actual NSDI experiments, such as focal averaging and integration over the perpendicular momentum components, which are not well resolved, tend to wash out quantum features such as interference [34, 35]. There is another pathway to double ionization, which is known to be especially relevant in the below-threshold-intensity region (where the maximal kinetic energy upon return is below the ionization potential of the singly charged ion). In this scenario, in the collision the second electron is pumped into an excited state from where it is subsequently liberated by the laser field. This pathway was dubbed recollision-excitation with subsequent ionization (RESI). Usually, depending on the laser parameters, only a few excited ionic states contribute to this process. Hence, it can be expected that the effect of interference could be more easily observed for this pathway. If identified, it will provide opportunities to probe or control the excited-state dynamics in the intense laser field.

We should remark that in the below-threshold intensity region, the electron-momentum-correlation distribution (EMCD) of the Ar atom shows a transition from anti-correlation to correlation with increasing laser intensity [36], which may be attributed to interference between different RESI channels [37] or to a multiple-rescattering process [38]. Moreover, recent analysis indicates that interference in the RESI process may lead to a change of the EMCD with increasing pulse duration [39]. However, no decisive conclusion has been reached for these phenomena yet.

Here we report clear evidence of quantum interference, arising from the RESI pathway in NSDI of the xenon atom subject to a mid-infrared laser field. The identification of quantum interference has been made possible by a careful inspection of the intensity dependence of the EMCD, for which both RII and RESI contribute.

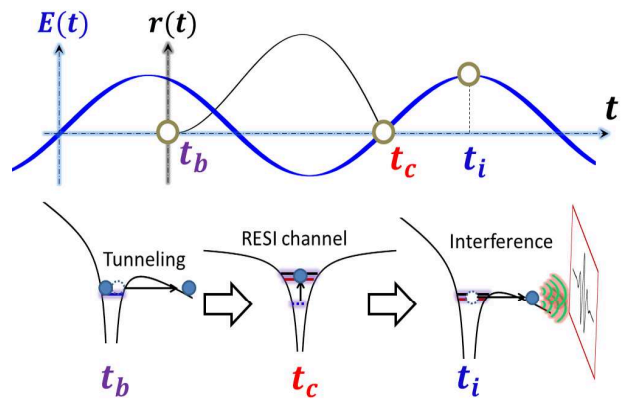


FIG. 1: (color online) Picture of the ionization pathways of RESI. The blue thick horizontal arrow indicates the time axis. The blue curve denotes the laser electric field. As time evolves, one of the valence electrons is liberated through tunneling at  $t_b$ . This electron is accelerated into a recollision with the core at the time  $t_c$  when there are two pathways: (i) it will knock out the other electron to induce double ionization (RII) (not shown here); (ii) it will pump the core into one of several excited states and the excited core will be further ionized by the laser electric field (RESI) at  $t_i$ . One typical rescattering orbit is indicated by the black curve. The electron wavepackets from different excited-core channels will interfere, which leads to an oscillation of the intensity dependence of the asymmetry parameter of the EMCD, see text for details. The 3 pictures in the lower part depict three key steps of the physical process in question.

For the RESI pathway, the second electron may arrive in the same final state through different intermediate ionic excited states, see Fig. 1. The interference between different excitation channels will give rise to a distinct intensity-dependent feature revealed in the experiment. By disentangling the contributions of the RII and the RESI pathways in our analysis, the effect of quantum interference in the RESI pathway becomes obvious.

## II. RESULTS

The experiments have been performed for Xe subject to intense midinfrared laser field at 2400nm with cold target recoil-ion momentum spectroscopy (COLTRIMS) [40–42]. The mid-infrared laser field employed in our experiments is generated from a commercial OPA laser system (TOPAS-C, Light Conversion, Inc.), which is pumped by a Ti:Sapphire femtosecond laser system (Legend, Coherent, Inc.) with a repetition rate of 1 kHz at 800 nm. Before the laser beam is directed into a newly-built COLTRIMS, the laser pulse energy is precisely controlled with a combination of a broadband achromatic  $\lambda/2$  plate and a broadband thin-film polarizer. The laser beam is focused with a concave mirror inside the vacuum

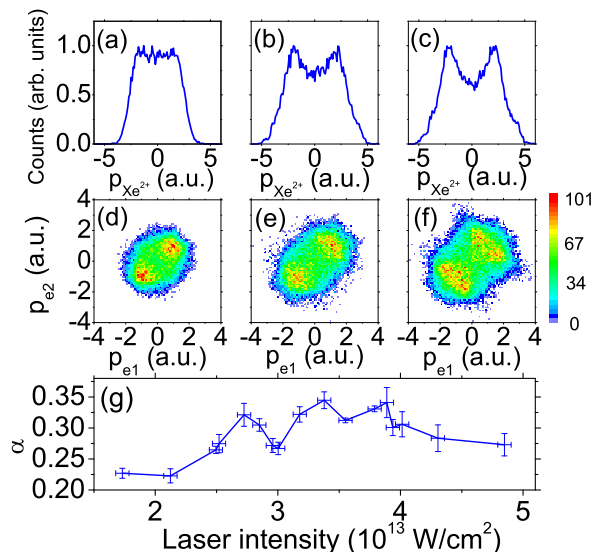


FIG. 2: (color online) Measured longitudinal momentum distributions of the  $\text{Xe}^{2+}$  ion ((a)(b)(c)) and the EMCs ((d)(e)(f)) from NSDI of Xe by a linearly polarized laser field at 2400 nm. The laser intensities are: (a)(d)  $I = 1.7 \times 10^{13}$  W/cm<sup>2</sup>; (b)(e)  $I = 3.2 \times 10^{13}$  W/cm<sup>2</sup>; (c)(f)  $I = 4.8 \times 10^{13}$  W/cm<sup>2</sup>. Measured asymmetry parameter  $\alpha$  as a function of the laser intensity for NSDI of Xe at 2400 nm (g).

chamber and the atomic supersonic beam is irradiated by the intense laser field in the focus. The created photoelectrons and photoions are accelerated by a uniform weak electric field (around 13.8 V/cm) towards Microchannel Plate (MCP) detectors equipped with delay line anodes (HEX75 and DLD80, RoentDek Handels GmbH, for electrons and ions, respectively). From the impact positions and times-of-flight resolved by the detectors, the three-dimensional momenta of both fragments can be retrieved. A weak uniform magnetic field (around 4.7 Gauss) generated by a pair of Helmholtz coils is applied to confine the electron movement perpendicular to the electric field. The earth magnetic field is compensated with two pairs of auxiliary coils. A varied pinhole, which can be tuned with four micrometer drivers outside the vacuum chamber, is employed to reduce the intersection of the supersonic beam and therefore the production rate of photofragments when necessary. The laser intensities are determined with a procedure utilizing the photoelectron momentum distribution from ionization of atoms subject to a close-to-circularly polarized laser field, where nonadiabatic effects are considered [43]. During the measurement, great attention is paid to keep the production rate of photofragments below 20% of the repetition rate, which ensures that less than one ionization event occurs for each pulse. The false coincidence from the background is estimated to be around 6%.

The measured longitudinal-momentum distributions of the  $\text{Xe}^{2+}$  ion are shown in Figs. 2(a)-(c). A pronounced monotonic transition from a flat-top to a broad double-

hump structure with a well developed minimum at zero momentum is observed when the laser intensity is increased from  $I = 1.7 \times 10^{13}$  W/cm<sup>2</sup> (see Fig. 2(a)) to  $I = 4.8 \times 10^{13}$  W/cm<sup>2</sup> (see Fig. 2(c)). This feature can be attributed to the contribution of RII, which increases with increasing return energy of the returning electron. In detail, the results can be well understood by considering the energy dependence of the cross sections of electron impact ionization and excitation [44, 45].

For further study of NSDI of Xe, the EMCs are also measured. The typical results are shown in Figs. 2(d)-(f). Similar to other noble gases [29–31], the EMCs for this long wavelength show a pattern typical of the NSDI process: two symmetrical maxima in the 1st and 3rd quadrants at momenta far from zero. This is in contrast to the distributions at 800 nm, which show a sequential feature [29] over a wide range of intensity: symmetrical distributions with respect to the maximum (at the origin) in all four quadrants [46]. At low intensities (see Fig. 2(d)), the momentum distributions are concentrated in the 1st and 3rd quadrants along the main diagonal meaning that both electrons are emitted into the same hemisphere with similar longitudinal momenta. As discussed extensively [29, 47], this electron correlation is characteristic of the RII pathway. However, some events in this figure can be attributed to the RESI pathway, where excited states are involved during ionization. In contrast to RII, electrons liberated by the RESI mechanism are found in all four quadrants [36, 47–49]. Since RII events are mainly concentrated in the 1st and 3rd quadrants, the yields in the 2nd and 4th quadrants should reflect the RESI contribution. With increasing intensity, the distributions in the 1st and 3rd quadrants cover larger and larger areas, with distinct off-diagonal structures [see Figs. 2(e) and 2(f)], which are close to the situation at 3.1  $\mu\text{m}$  [50].

To shed more light on the intensity dependence of the EMCs, we extract the difference between the total yields in the 1st and 3rd quadrants and those in the 2nd and 4th quadrants and express it through the asymmetry parameter  $\alpha = (Y_{1\&3} - Y_{2\&4}) / (Y_{1\&3} + Y_{2\&4})$ , where  $Y_{1\&3}$  and  $Y_{2\&4}$  denote the yields in the 1st and 3rd quadrants and those in the 2nd and 4th quadrants, respectively. Recall that, within the rescattering scenario, correlated electron pairs, which populate the first and third quadrants (i.e., the final momenta have the same sign), are usually attributed to the RII pathway. On the other hand, the anticorrelated electron pairs, which populate the second and fourth quadrants (i.e., the final momenta have opposite signs), are associated with the RESI pathway. This asymmetry parameter allows for a quantitative comparison of the contributions from RII and RESI pathways [51]. This in turn enables one to extract substantial quantum aspects in the NSDI process [37, 39], which are usually masked by the experimental complexities, such as focal averaging, etc. The intensity dependence of  $\alpha$  is presented in Fig. 2(g), which exhibits a remarkably pronounced fast oscillation on top of a smooth background.

### III. DISCUSSION

What is the physics behind this oscillation structure? One possible mechanism appears to be resonance between bound states similar to the Freeman resonances in the ATI process. However, this can be ruled out by considering that, for a laser wavelength of 2400 nm, the intensity change corresponding to the ponderomotive-energy change  $\Delta U_p = \omega$  is only about  $1 \text{ TW/cm}^2$ , which is much smaller than the period (about  $5 \sim 10 \text{ TW/cm}^2$ ) of the oscillation shown in Fig. 2(g).

To understand the physics behind the oscillation, we first perform a calculation based on the semiclassical model. The calculation procedure is based on a well-verified numerical method, which has been employed successfully to understand many aspects of the NSDI process, e.g., the knee structure in the distribution of the yield of double-charged ions versus intensity; the maxima in the 1st and 3rd quadrants of the EMCD *etc.* [52–55].

In this model [52–56], one electron is released at the outer edge of the field-suppressed Coulomb potential through tunneling with a rate given by the ADK formula [57]. The subsequent evolution of the tunneled and the bound electron is determined by Newton's equation of motion (in atomic units,  $e = m = \hbar = 1$ )

$$d^2 \mathbf{r}_i / dt^2 = -\mathbf{E}(t) - \nabla (V_{ne}^i + V_{ee}). \quad (1)$$

Here,  $i = 1, 2$  denote the tunneled and the initially bound electrons with ionization potentials  $I_{p1}$  and  $I_{p2}$ , respectively. The laser field  $\mathbf{E}(t) = f(t)E_0 \sin \omega t \hat{\mathbf{z}}$  is linearly polarized in the  $z$  direction and has a cosine square envelope. The Coulomb potentials are  $V_{ne}^i = -Z_{\text{eff}}/|\mathbf{r}_i|$  and  $V_{ee} = 1/|\mathbf{r}_1 - \mathbf{r}_2|$ , where  $Z_{\text{eff}} = \sqrt{2I_{p2}}$  is the effective charge of the  $\text{Xe}^{2+}$  ion and  $\mathbf{r}_i$  the position vector of the  $i$ th electron with respect to the nucleus.

In order to solve Eq. (1), we have to determine the initial conditions of the two electrons. Assuming the quasi-static approximation is valid for the tunneled electron, its initial conditions can be obtained. The tunneling process can be described in parabolic coordinates by the Schrödinger equation [58, 59]

$$\frac{d^2 \phi}{d\eta^2} + \left( \frac{I_{p1}}{2} + \frac{2 - \sqrt{2I_{p1}}}{2\eta} + \frac{1}{4\eta^2} + \frac{E\eta}{4} \right) \phi = 0. \quad (2)$$

Equation (2) describes the tunneling process for a single electron with energy  $K = I_{p1}/4$  within a one-dimensional effective potential  $U(\eta) = -(2 - \sqrt{2I_{p1}})/4\eta - 1/8\eta^2 - E\eta/8$  where  $E$  is the uniform external field. At some time  $t_0$  while the pulse is on, the first electron tunnels out of the effective potential  $U(\eta)$  at its turning point  $\eta_0$ , which is determined by  $U(\eta) = K$ . The initial velocities are set to be  $v_z = 0$ ,  $v_x = v_{\perp} \cos \theta$ , and  $v_y = v_{\perp} \sin \theta$ , where  $v_{\perp}$  is the transverse velocity,  $\theta$  is the angle between  $v_{\perp}$  and the  $x$  axis. The weight of each trajectory is evaluated by  $w(t_0, v_{\perp}) = w(0)\bar{w}(1)$  [57], where

$$w(0) = \frac{4(2I_{p1})^2}{E} \exp\left(-\frac{2}{3E}(2I_{p1})^{3/2}\right), \quad (3)$$

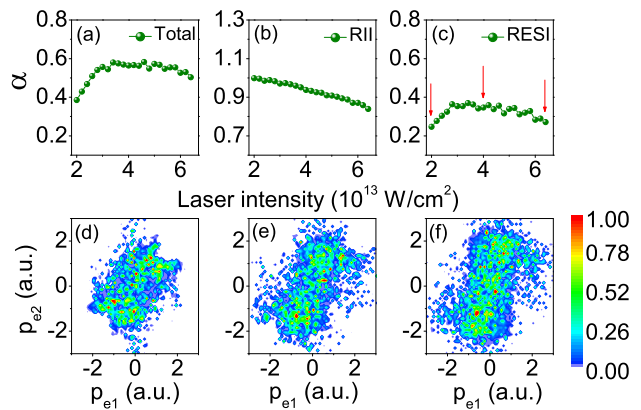


FIG. 3: (color online) Semiclassical simulation results corresponding to the experimental results of Fig. 2. The calculated asymmetry parameter  $\alpha$  includes (a) all DI events, (b) only RII events, (c) only RESI events. The EMCDs in (d),(e), and (f) are calculated for RESI at (d)  $2.0 \times 10^{13} \text{ W/cm}^2$ ; (e)  $4.0 \times 10^{13} \text{ W/cm}^2$ ; (f)  $6.0 \times 10^{13} \text{ W/cm}^2$ . These intensities are indicated by the red arrows in panel (c).

$$\bar{w}(1) = \frac{(2I_{p1})^{1/2}}{E\pi} \exp\left(-\frac{v_{\perp}^2 (2I_{p1})^{1/2}}{E}\right). \quad (4)$$

The bound electron is initially in the ground state of the  $\text{Xe}^+$  ion, and its initial distribution is approximated by a micro-canonical distribution [60].

The calculated results based on the above semiclassical model are presented in Fig. 3. If all DI events are included, as shown in Fig. 3(a), the asymmetry parameter  $\alpha$  shows a smooth hump structure, which is qualitatively consistent with the measurements (see Fig. 2(g)) except that the distinct oscillation on top of the hump is absent. Some very small oscillations that may be identified in Fig. 3(a) can be attributed to fluctuations in the Monte-Carlo simulation. Generally, in the semiclassical model, the contributions from RII and RESI can be distinguished by the time interval  $\Delta t$  between the collision time and the ionization time. If  $\Delta t < 0.1T$  ( $T$  is the optical cycle), the DI event can be envisioned as a RII event, otherwise as a RESI event. Here we calculate the asymmetry parameters for both cases separately and also for the total. The procedure is analogous to that applied in Fig. 2, where the asymmetry parameter (in Fig. 2(g)) is extracted from the measured EMCDs [e.g., Figs. 2(d), 2(e), and 2(f)]. (Note that Figs. 3 (d)-(f) only display the EMCDs for the RESI pathway.) The asymmetry parameter of the RII process (see Fig. 3(b)) decreases monotonically while for the RESI process (Fig. 3(c)) it shows a hump similar to Fig. 2(g). This result gives us a hint that the hump structure may mainly come from the events with  $\Delta t > 0.1T$ , i.e., the RESI pathway.

The above behavior of the calculated asymmetry parameters for  $\Delta t < 0.1T$  and  $\Delta t > 0.1T$  can be understood as follows. For each electron in an event of

$\Delta t < 0.1T$ , its final momentum is the sum of its residual momentum right after the recollision and the drift momentum due to the subsequent acceleration in the laser field. Calculation shows that, since the DI events are mainly induced by forward scattering provided only the orbits with single-return collision are considered, the residual momenta and the drift momenta tend to cancel each other [61]. Although both the residual momentum and the drift momentum increase with increasing laser intensity, the residual momentum grows faster, which results in a smaller final momentum and even a reversal of its direction. Note that the residual momentum is usually smaller than the drift momentum at low intensity. Therefore, the areas covered by the electrons in the EMCD become larger and move closer to the origin. Hence, with increasing intensity, more and more population coming from events with  $\Delta t < 0.1T$  spills over into the 2nd and 4th quadrants, This gives rise to the monotonic decrease of the asymmetry parameter with rising laser intensity [61].

In contrast, for the RESI events with  $\Delta t > 0.1T$ , the intensity dependence of the momentum distributions is different for the two electrons. The first electron is in the same situation as discussed above for  $\Delta t < 0.1T$ . However, the second electron is liberated with no residual momentum: its final momentum is only determined by the drift momentum. Therefore, with increasing intensity, the momentum of the first electron becomes smaller, while that of the second one becomes larger, which will cause the momentum distribution in the case of  $\Delta t > 0.1T$  to move i) toward the vertical axis and ii) away from the origin, as shown by Figs. 3(d), 3(e) and 3(f). It should be noted that no symmetrization is applied in Fig. 3. In fact, i) and ii) have opposite effects on the asymmetry parameter and one or the other may dominate depending on the laser intensity. At low intensity, e.g.,  $2 \times 10^{13}$  W/cm<sup>2</sup> where the momentum distributions are near the origin (see Fig. 3(d)), the effect of ii) dominates. With rising intensity, the electron distributions will move away from the origin and the asymmetry parameter will increase until  $I = 4 \times 10^{13}$  W/cm<sup>2</sup> (see Fig. 3(e)). At this intensity, the distributions are already very near the vertical axis and the effect of i) starts to dominate. If the intensity increases further, as shown in Fig. 3(f), the asymmetry parameter decreases. As a result, the evolution of the asymmetry parameter with respect to laser intensity for the RESI process (see Fig. 3(c)) shows a hump structure. This structure will persist even after the RII contributions are put in. The RII contribution will add a smooth decreasing background but not degrade the hump structure (see Fig. 3(c)).

We notice that, as discussed above, the pronounced oscillation on top of the measured hump is absent in the semiclassical simulation. This suggests that it has to be attributed to a quantum feature. To support this hypothesis, we employ the quantum-mechanical strong-field approximation (SFA) to simulate the NSDI process. The SFA theory has been very successful in explaining

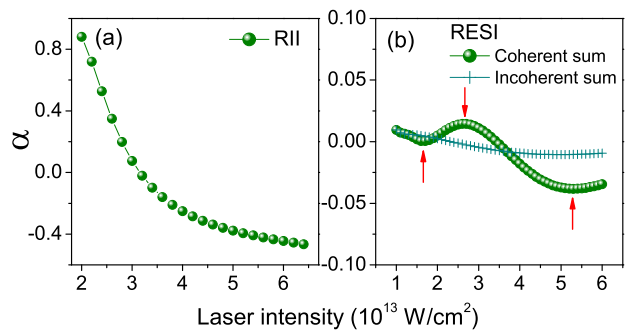


FIG. 4: (color online) The asymmetry parameters  $\alpha$  calculated with the SFA. (a) asymmetry parameter for the RII process; (b) asymmetry parameter for the RESI process. For the red arrows in panel (b), see the caption in Fig. 5.

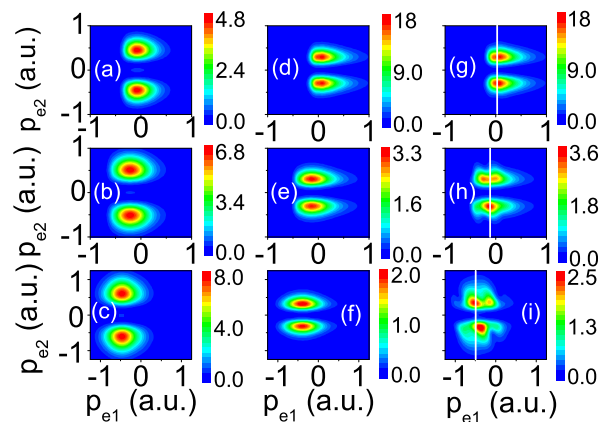


FIG. 5: (color online) EMCDs of the two electrons for RESI pathway based on the SFA calculation at three typical intensities, which are indicated by the red arrows in Fig. 4(b). (a), (d), and (g):  $1.7 \times 10^{13}$  W/cm<sup>2</sup>; (b), (e), and (h):  $2.6 \times 10^{13}$  W/cm<sup>2</sup>; (c), (f), and (i):  $5.3 \times 10^{13}$  W/cm<sup>2</sup>. (a)-(c):  $5p^45d$  channel; (d)-(f):  $5p^46s$  channel; (g)-(i): coherent sum of the two channels.

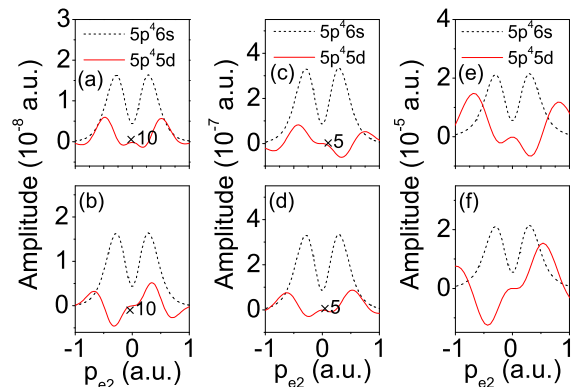


FIG. 6: (color online) Real part (the first row) and imaginary part (the second row) of the transition amplitude vs momentum of the second electron at different intensities. See the text for more details. (a) and (b):  $1.7 \times 10^{13}$  W/cm<sup>2</sup>; (c) and (d):  $2.6 \times 10^{13}$  W/cm<sup>2</sup>; (e) and (f):  $5.3 \times 10^{13}$  W/cm<sup>2</sup>.

basic features of the NSDI process, e.g., it is capable of predicting quantum interference effects [37, 39, 62]. In the frame of the SFA, RII can be described as a three-step process: in the first step, the first (initially bound) electron is promoted by the laser field to a Volkov state. In the second step, the first electron interacts with the second (up to this time still bound) electron via their repulsive Coulomb potential. In the final step both electrons are described by Volkov states while they travel towards the detector. To describe the RESI process, a fourth step has to be added. Namely, the recolliding first electron does not immediately liberate the second electron, but only promotes it to an excited state, from which it is freed by the laser field at a later time. In the RESI process, the second electron may acquire the same final momentum through different intermediate ionic excited states, and these excitation channels may interfere with each other [37]. To include the interference between different ionic excitation channels, two excited states ( $5p^45d$  and  $5p^46s$ ) are taken into account in our calculation. In addition, depletion of the excited state is also included in our model [37].

Our calculations are based on the length-gauge strong-field approximation. The transition amplitude of the RII process is (atomic units  $m = \hbar = e = 1$  are used) [63]

$$\begin{aligned}
M^{\text{RII}}(\mathbf{p}_1, \mathbf{p}_2) &= \int_{-\infty}^{\infty} dt \int_{-\infty}^t dt' \int d^3\mathbf{k} \\
&\times \langle \psi_{\mathbf{p}_1}^{(V)}(t) \psi_{\mathbf{p}_2}^{(V)}(t) | V_{12} | \psi_{\mathbf{k}}^{(V)}(t) \psi_g^{(2)}(t) \rangle \\
&\times \langle \psi_{\mathbf{k}}^{(V)}(t') | V_1 | \psi_g^{(1)}(t') \rangle
\end{aligned} \quad (5)$$

where  $|\psi_g^{(i)}(t)\rangle$  is the ground state of the  $i$ th electron,  $|\psi_{\mathbf{p}}^{(V)}(t)\rangle$  the Volkov state with asymptotic momentum  $\mathbf{p}$ ,  $V_1$  denotes the binding potential of the first electron, and  $V_{12}$  is the interaction between the two electrons.

The transition amplitude of the RESI process for the excitation channel  $j$  is, taking into account depletion [37, 48]

$$\begin{aligned}
M_j^{\text{RESI}}(\mathbf{p}_1, \mathbf{p}_2) &= \int_{-\infty}^{\infty} dt \int_{-\infty}^t dt' \int_{-\infty}^{t'} dt'' \int d^3\mathbf{k} \\
&\times \exp\left(-\int_{t'}^t \gamma_j \sin^2 \omega\tau d\tau / 2\right) \langle \psi_{\mathbf{p}_2}^{(V)}(t) | V_2 | \psi_j^{(2)}(t) \rangle \\
&\times \langle \psi_{\mathbf{p}_1}^{(V)}(t') \psi_j^{(2)}(t') | V_{12} | \psi_{\mathbf{k}}^{(V)}(t') \psi_g^{(2)}(t') \rangle \\
&\times \langle \psi_{\mathbf{k}}^{(V)}(t'') | V_1 | \psi_g^{(1)}(t'') \rangle,
\end{aligned} \quad (6)$$

where the depletion rate of the excited state is approximately described as  $\gamma_j \sin^2 \omega t / 2$ , with the decay rate  $\gamma_j$  calculated from a numerical solution of the time-dependent Schrödinger equation for each excited state. The ket  $|\psi_j^{(2)}(t)\rangle$  is the excited state of the second electron and  $V_2$  denotes the binding potential of the second

electron in the excited state. In our calculation  $V_1$ ,  $V_2$ , and  $V_{12}$  are given by

$$V_i = -\frac{Z_i^{\text{eff}}}{r_i}, \quad V_{12} = \frac{1}{|\mathbf{r}_1 - \mathbf{r}_2|}, \quad (7)$$

where  $Z_i^{\text{eff}} = n\sqrt{2I_{pi}^{\text{eff}}}$  is the effective charge of the  $i$ th electron,  $n$  is the principal quantum number of the bound state, and  $I_{pi}$  the respective ionization potential of the  $i$ th electron.

The multiple integrals in Eqs. (5) and (6) are solved using saddle-point methods. The corresponding saddle-point equations for the RII process are

$$[\mathbf{k} + \mathbf{A}(t')]^2 = -2I_{p1}, \quad (8)$$

$$[\mathbf{p}_1 + \mathbf{A}(t)]^2 + [\mathbf{p}_2 + \mathbf{A}(t)]^2 = [\mathbf{k} + \mathbf{A}(t)]^2 - 2I_{p2}, \quad (9)$$

$$\int_{t'}^t d\tau [\mathbf{k} + \mathbf{A}(\tau)] = 0, \quad (10)$$

and for the RESI process

$$[\mathbf{k} + \mathbf{A}(t'')]^2 = -2I_{p1}, \quad (11)$$

$$[\mathbf{p}_1 + \mathbf{A}(t')]^2 = [\mathbf{k} + \mathbf{A}(t')]^2 - 2(I_{p2} - I_{p2j}), \quad (12)$$

$$\int_{t''}^{t'} d\tau [\mathbf{k} + \mathbf{A}(\tau)] = 0, \quad (13)$$

$$[\mathbf{p}_2 + \mathbf{A}(t)]^2 = -2I_{p2j}. \quad (14)$$

Equations (8) and (11) describe the tunneling process of the first electron, Eqs. (9) and (12) give the energy conserving condition, Eqs. (10) and (13) express the return of the first electron to its parent, and Eq. (14) describes the tunneling process of the second electron from its excited state. Due to depletion, here we only take into account the orbit whose ionization time  $t$  is later than and closest to the collision time  $t'$ .

**Table 1:** The configurations of the dominant channels.

Channel	$I_p$ (a.u.)	Configuration
1	0.345	$5s^25p^45d$
2	0.19	$5s^25p^46s$

The wavefunctions used in our calculation are obtained numerically based on the method in Ref. [64]. In our calculation, only the states with zero magnetic quantum number are taken into account due to the linear polarization of the laser field. In the calculation of the RESI process, two excitation channels of  $\text{Xe}^+$  are enough to

produce a result qualitatively consistent to measurement. Their configurations are listed in Table 1. It should be noted that the excited state  $5p^45d$  is a pure  $5d$  state, while the state  $5p^46s$  contains an about 10-percent  $6d$  admixture in addition to the dominant  $6s$  component.

The asymmetry parameters of the RII and RESI processes calculated via the SFA are shown in Figs. 4(a) and 4(b), respectively. The asymmetry parameter of RII shows a smooth decreasing trend similar to the corresponding semiclassical result in Fig. 3(b) though it drops much faster and even turns negative. The difference is due to the underestimate of the contributions of the long orbits (the travel time between the tunneling ionization time and the rescattering time is longer than one optical cycle) by the SFA [61]. The long orbits always contribute to the 1st and 3rd quadrants in the EMCD, since the momenta of the long orbits increase much more slowly with increasing laser intensity, in contrast to those of the shortest orbit.

Satisfactorily, if the contributions of the two ionic excitation channels are summed coherently, according to Fig. 4(b) the asymmetry parameter of the RESI process shows a very clear oscillation, which is qualitatively close to the experimental result in Fig. 2(g). However, if the contributions of the two channels are summed incoherently, the oscillation disappears. Therefore, the oscillation can be attributed to the interference between different ionic excitation channels.

To provide further insight into the interference mechanism behind the oscillation, in Fig. 5 we present the EMCDs for the two ionic excitation channels and their coherent sum at 3 typical laser intensities (the corresponding laser intensities are indicated in Fig. 4(b) with red arrows). In the calculation, we restrict ionization of the first electron to the first half optical cycle of the laser field. To simplify the analysis, no symmetrization procedure is applied to any of the calculated EMCDs in Fig. 5. The figure demonstrates that the shape of the momentum distributions varies with channel and intensity. The momentum distributions in Figs. 5(d)-(f) show a  $6d$ -like shape rather than a  $6s$ -like shape (the  $s$  state usually has a cross-like shape with the distribution mainly on the axes; see, for example, Ref. [39]). The reason is that, with the numerical wavefunction employed in our calculation, the excited state of  $5p^45d$  can be taken as a pure  $5d$  state, while the state of  $5p^46s$  contains about 10-percent  $6d$  component in addition to the dominant  $6s$  component. Although the percentage of  $6d$  component is small, it makes the dominant contribution to the double ionization in the  $5p^46s$  channel due to its much larger cross section compared with the  $6s$  component.

Generally, for each individual ionic excitation channel, the EMCD is symmetric with respect to the  $p_{e2} = 0$  axis. But once the two channels are summed coherently, the above symmetry of the EMCD is broken. At the intensity of  $1.7 \times 10^{13}$  W/cm<sup>2</sup> (see Fig. 5(g)), the interference effect is not obvious: due to the relatively small amplitude of the  $5p^45d$  state, the difference between the upper

( $p_{e2} > 0$ ) and lower ( $p_{e2} < 0$ ) parts of the distribution can only be seen after integration as shown in Fig. 4(b) where the asymmetry parameter shows a minimum. When the intensity increases to  $2.6 \times 10^{13}$  W/cm<sup>2</sup>, the interference effect becomes evident and a bright spot arises in the lower part of the distribution (the third quadrant) while the distribution in the upper part (the second quadrant) is reduced as can be seen in Fig. 5(h). When the intensity increases further to  $5.3 \times 10^{13}$  W/cm<sup>2</sup>, the distribution in the upper part is significantly enhanced and two maxima appear. Therefore, when the intensity increases, the asymmetry parameter oscillates, alternatingly enhanced by constructive interference and suppressed by destructive interference (see Fig. 4(b)).

The above interference effect is rooted in the phases of the two contributing channels, which are intensity dependent. To see this more clearly, in Fig. 6 we plot the real and imaginary parts of the transition amplitudes  $M_j$  of the two channels with  $j = 1, 2$  ( $j = 1$  corresponds to the  $5p^45d$  state and  $j = 2$  corresponds to the  $5p^46s$  state) at different intensities. For simplicity, we have extracted the phase of channel 2, i.e., we plot the real and imaginary parts of  $|M_j|e^{i(\varphi_j - \varphi_2)}$ , where  $\varphi_j$  is the phase of the transition amplitude  $M_j$ . The momentum of the first electron is fixed while the momentum of the second electron varies along the white lines in Figs. 5(g)-(i) (here only momenta with zero transverse components are considered since the differential ionization rate decreases fast with increasing transverse momentum).

Figure 6 clearly pinpoints the origin of the interference. Since the amplitude of channel 1 is very small compared with channel 2 at low laser intensities, for visual convenience the amplitude of channel 1 is multiplied by factors of 10 and 5 at the intensities of  $1.7 \times 10^{13}$  W/cm<sup>2</sup> and  $2.6 \times 10^{13}$  W/cm<sup>2</sup>, respectively. At the lowest intensity of  $1.7 \times 10^{13}$  W/cm<sup>2</sup>, for positive momentum the two channels interfere constructively both in the real and the imaginary part, while for negative momentum there is marked destructive interference between the two channels in the imaginary part. At the intermediate intensity, the situation reverses. The destructive interference appears at positive momentum in the real part of the amplitude while all the other parts show a constructive interference. It is interesting that the situation reverses again at the highest intensity of  $5.3 \times 10^{13}$  W/cm<sup>2</sup>: the destructive interference moves back to negative momentum in the imaginary part. As a result, after integration over the momentum, the above intensity-dependent interference leads to the oscillation of the asymmetry parameters shown in Fig. 4.

It should be mentioned that thus far the SFA calculation results cannot be quantitatively compared to the measurements. This can be attributed to the fact that the SFA model neglects the influence of the ionic Coulomb potential on the photoelectron [61] and also the influence of the external field on the excited states. In addition, many excited states could be involved in the ionization process. To make the calculation capacity within

our reach, at this stage we only considered the simplest situation that two excited states are involved. Therefore, only a qualitative description of the oscillation can be achieved in the present theory. However, our analysis indicates that the interference between different channels in the RESI process can indeed give rise to an oscillatory intensity dependence of the asymmetry parameter, which is beyond the scope of the semiclassical picture of the NSDI process. The detailed structure, i.e., the intensities where the peaks occur and their separations *etc.*, differs from the experimental data. This is not a surprise since only a qualitative description of the oscillation can be achieved in the present theory, as explained above. Thus a much more elaborate theory is still required to provide a quantitative description of the experimental results presented here.

#### IV. CONCLUSION

To conclude, we report the experimental observation of a pronounced oscillation in the asymmetry of the electron-electron momentum correlation of nonsequential double ionization of xenon in a 2400-nm laser field upon variation of the laser intensity. Namely, the population of the 2nd and 4th quadrants of the EMCD (the two electrons emitted back to back) oscillates with respect to that in the 1st and 3rd quadrants (the two electrons emitted side by side) if the laser intensity increases. We performed semiclassical simulations, which reproduced the overall shape of the asymmetry parameter, but not the oscillation. This suggests that the oscillation can be attributed to the contribution of a quantum process. On the basis of simulations using the quantum-mechanical strong-field approximation, we attribute this oscillation

to the interference between ionization channels from different intermediate ionic excited states in the RESI pathway. Our work provides an experimental fingerprint that interference plays an important role in the NSDI process. This interference effect in NSDI may also be present in other experimental schemes, and, for example, it could be interesting to see how the oscillation in the asymmetry manifests itself for the bicircular laser fields [65, 66].

Looking forward, interference-related effects may provide a new avenue to image the ultrafast electron dynamics in an intense laser field. Compared to the relatively well established presence of interference in ATI or HHG, for NSDI we are confronted with a completely new situation: the RESI pathway, which introduces a nonzero time difference between recollision and second ionization, allows one to image the ultrafast evolution of the excited electronic wavepackets in atomic or molecular ions. This is especially important for molecular systems, for which the excited states will evolve while the nuclei are moving. One could employ, e.g., laser pulses with different wavelengths, such as in the “molecular clock” scheme [67], to probe and manipulate the correlated dynamics of the nuclei and the excited states of the molecular ions through the interference arising from the RESI pathway.

#### ACKNOWLEDGMENTS

This work is supported by the National Basic Research Program of China (No. 2013CB922201), the National Key Program for S&T Research and Development (No. 2016YFA0401100), the National Natural Science Foundation of China (Nos. 11334009, 11374329, 11425414 and 11474321), the Strategic Priority Research Program of the Chinese Academy of Sciences (No. XDB21010400).

- 
- [1] P. Salières, B. Carré, L. Le Déroff, F. Grasbon, G. G. Paulus, H. Walther, R. Kopold, W. Becker, D. B. Milošević, A. Sanpera, and M. Lewenstein, *Science* **292**, 902 (2001).
  - [2] M. P. Hertlein, P. H. Bucksbaum, and H. G. Muller, *J. Phys. B* **30**, L197 (1997).
  - [3] P. Hansch, M. A. Walker, and L. D. Van Woerkom, *Phys. Rev. A* **55**, R2535 (1997).
  - [4] H. G. Muller, and F. C. Kooiman, *Phys. Rev. Lett.* **81**, 1207 (1998).
  - [5] F. Lindner, M. G. Schätzel, H. Walther, A. Baltuška, E. Goulielmakis, F. Krausz, D. B. Milošević, D. Bauer, W. Becker, and G. G. Paulus, *Phys. Rev. Lett.* **95**, 040401 (2005).
  - [6] W. Quan, X. Y. Lai, Y. J. Chen, C. L. Wang, Z. L. Hu, X. J. Liu, X. L. Hao, J. Chen, E. Hasović, M. Busuladžić, W. Becker, and D. B. Milošević, *Phys. Rev. A* **88**, 021401(R) (2013).
  - [7] A. Talebpour, C.-Y. Chien, and S. L. Chin, *J. Phys. B* **29**, L677 (1996).
  - [8] C. Guo, M. Li, J. P. Nibarger, and G. N. Gibson, *Phys. Rev. A* **58**, R4271 (1998).
  - [9] J. Muth-Böhm, A. Becker, and F. H. M. Faisal, *Phys. Rev. Lett.* **85**, 2280 (2000).
  - [10] Z. Y. Lin, X. Y. Jia, C. L. Wang, Z. L. Hu, H. P. Kang, W. Quan, X. Y. Lai, X. J. Liu, J. Chen, B. Zeng, W. Chu, J. P. Yao, Y. Cheng, and Z. Z. Xu, *Phys. Rev. Lett.* **108**, 223001 (2012).
  - [11] M. Busuladžić, A. Gazibegović-Busuladžić, D. B. Milošević, and W. Becker, *Phys. Rev. Lett.* **100**, 203003 (2008).
  - [12] M. Okunishi, R. Itaya, K. Shimada, G. Prümper, K. Ueda, M. Busuladžić, A. Gazibegović-Busuladžić, D. B. Milošević, and W. Becker, *Phys. Rev. Lett.* **103**, 043001 (2009).
  - [13] H. Kang, W. Quan, Y. Wang, Z. Lin, M. Wu, H. Liu, X. Liu, B. B. Wang, H. J. Liu, Y. Q. Gu, X. Y. Jia, J. Liu, J. Chen, and Y. Cheng, *Phys. Rev. Lett.* **104**, 203001 (2010).
  - [14] M. Lein, N. Hay, R. Velotta, J. P. Marangos, and P. L. Knight, *Phys. Rev. Lett.* **88**, 183903 (2002).
  - [15] T. Kanai, S. Minemoto, and H. Sakai, *Nature* **435**, 470

- (2005).
- [16] C. Vozzi, F. Calegari, E. Benedetti, J.-P. Caumes, G. Sansone, S. Stagira, M. Nisoli, R. Torres, E. Heesel, N. Kajumba, J. P. Marangos, C. Altucci and R. Velotta, *Phys. Rev. Lett.* **95**, 153902 (2005).
- [17] B. K. McFarland, J. P. Farrell, P. H. Bucksbaum, and M. Gühr, *Science* **322**, 1232 (2008).
- [18] O. Smirnova, Y. Mairesse, S. Patchkovskii, N. Dudovich, D. Villeneuve, P. Corkum, and M. Yu. Ivanov, *Nature* **460**, 972 (2009).
- [19] W. Becker, F. Grasbon, R. Kopold, D. B. Milošević, G. G. Paulus, and H. Walther, *Adv. At. Mol. Opt. Phys.* **48**, 35 (2002).
- [20] Y. Huismans, A. Gijsbertsen, A. S. Smolkowska, J. H. Jungmann, A. Rouzée, P. S. W. M. Logman, F. Lépine, C. Cauchy, S. Zamith, T. Marchenko, J. M. Bakker, G. Berden, B. Redlich, A. F. G. van der Meer, M. Yu. Ivanov, T.-M. Yan, D. Bauer, O. Smirnova, and M. J. J. Vrakking, *Phys. Rev. Lett.* **109**, 013002 (2012).
- [21] T. Marchenko, Y. Huismans, K. J. Schafer, and M. J. J. Vrakking, *Phys. Rev. A* **84**, 053427 (2011).
- [22] W. Yang, Z. Sheng, X. Feng, M. Wu, Z. Chen, and X. Song, *Opt. Express* **22**, 2519 (2014).
- [23] X. B. Bian, and A. D. Bandrauk, *Phys. Rev. Lett.* **108**, 263003 (2012).
- [24] J. Itatani, J. Levesque, D. Zeidler, H. Niikura, H. Pépin, J. C. Kieffer, P. B. Corkum, and D. M. Villeneuve, *Nature* **432**, 867 (2004).
- [25] C. Vozzi, M. Negro, F. Calegari, G. Sansone, M. Nisoli, S. De Silvestri, and S. Stagira, *Nature Phys.* **7**, 822 (2011).
- [26] W. Li, X. Zhou, R. Lock, S. Patchkovskii, A. Stolow, H. C. Kapteyn, and M. M. Murnane, *Science* **322**, 1207 (2008).
- [27] R. M. Lock, S. Ramakrishna, X. Zhou, H. C. Kapteyn, M. M. Murnane, and T. Seideman, *Phys. Rev. Lett.* **108**, 133901 (2012).
- [28] B. Walker, B. Sheehy, L. F. DiMauro, P. Agostini, K. J. Schafer, and K. C. Kulander, *Phys. Rev. Lett.* **73**, 1227 (1994).
- [29] Th. Weber, H. Giessen, M. Weckenbrock, G. Urbasch, A. Staudte, L. Spielberger, O. Jagutzki, V. Mergel, M. Vollmer, and R. Dörner, *Nature* **405**, 658 (2000).
- [30] C. Figueira de Morisson Faria, and X. Liu, *J. Mod. Opt.* **58**, 1076 (2011).
- [31] W. Becker, X. Liu, P. J. Ho, and J. H. Eberly, *Rev. Mod. Phys.* **84**, 1011 (2012).
- [32] K. C. Kulander, K. J. Schafer, J. L. Krause, in *Super-Intense Laser-Atom Physics* ed. B. Piraux, A. L'Huillier, and K. Rzażewski (Plenum, New York, 1993), p. 95.
- [33] P. B. Corkum, *Phys. Rev. Lett.* **71**, 1994 (1993).
- [34] R. Panfili, J. H. Eberly, and S. L. Haan, *Opt. Express* **8**, 431 (2001).
- [35] C. Figueira de Morisson Faria, X. Liu, A. Sanpera, and M. Lewenstein, *Phys. Rev. A* **70**, 043406 (2004).
- [36] Y. Liu, S. Tschuch, A. Rudenko, M. Dürr, M. Siegel, U. Morgner, R. Moshhammer, and J. Ullrich, *Phys. Rev. Lett.* **101**, 053001 (2008).
- [37] X. L. Hao, J. Chen, W. D. Li, B. Wang, X. Wang, and W. Becker, *Phys. Rev. Lett.* **112**, 073002 (2014).
- [38] Y. Q. Liu, D. Ye, J. Liu, A. Rudenko, S. Tschuch, M. Dürr, M. Siegel, U. Morgner, Q. Gong, R. Moshhammer, and J. Ullrich, *Phys. Rev. Lett.* **104**, 173002 (2010).
- [39] A. S. Maxwell, and C. Figueira de Morisson Faria, *Phys. Rev. Lett.* **116**, 143001 (2016).
- [40] J. Ullrich, R. Moshhammer, A. Dorn, R. Dörner, L. Ph. H. Schmidt, and H. Schmidt-Böcking, *Rep. Prog. Phys.* **66**, 1463 (2003).
- [41] T. Jahnke, Th. Weber, T. Osipov, A. L. Landers, O. Jagutzki, L. Ph. H. Schmidt, C. L. Cocke, M. H. Prior, H. Schmidt-Böcking, and R. Dörner, *J. Electron. Spectrosc. Relat. Phenom.* **141**, 229 (2004).
- [42] W. Quan, X. L. Hao, Y. J. Chen, S. G. Yu, S. P. Xu, Y. L. Wang, R. P. Sun, X. Y. Lai, C. Y. Wu, Q. H. Gong, X. T. He, X. J. Liu, and J. Chen, *Sci. Rep.* **6**, 27108 (2016).
- [43] W. Quan, M. H. Yuan, S. G. Yu, S. P. Xu, Y. J. Chen, Y. L. Wang, R. P. Sun, Z. L. Xiao, C. Gong, L. Q. Hua, X. Y. Lai, X. J. Liu, and J. Chen, *Opt. Express* **24**, 23248 (2016).
- [44] O. Herrwerth, A. Rudenko, M. Kremer, V. L. B. de Jesus, B. Fischer, G. Gademann, K. Simeonidis, A. Achteлик, Th. Ergler, B. Feuerstein, C. D. Schröter, R. Moshhammer, and J. Ullrich, *New J. Phys.* **10**, 025007 (2008).
- [45] Y. L. Wang, S. P. Xu, W. Quan, C. Gong, X. Y. Lai, S. L. Hu, M. Q. Liu, J. Chen, and X. J. Liu, *Phys. Rev. A* **94**, 053412 (2016).
- [46] X. Sun, M. Li, D. Ye, G. Xin, L. Fu, X. Xie, Y. Deng, C. Wu, J. Liu, Q. Gong, and Y. Liu, *Phys. Rev. Lett.* **113**, 103001 (2014).
- [47] B. Feuerstein, R. Moshhammer, D. Fischer, A. Dorn, C. D. Schröter, J. Deipenwisch, J. R. Crespo Lopez-Urrutia, C. Höhr, P. Neumayer, J. Ullrich, H. Rottke, C. Trump, M. Wittmann, G. Korn, and W. Sandner, *Phys. Rev. Lett.* **87**, 043003 (2001).
- [48] T. Shaaran, M. T. Nygren, and C. Figueira de Morisson Faria, *Phys. Rev. A* **81**, 063413 (2010).
- [49] D. F. Ye, and J. Liu, *Phys. Rev. A* **81**, 043402 (2010).
- [50] B. Wolter, M. G. Pullen, M. Baudisch, M. Sclafani, M. Hemmer, A. Senftleben, C. D. Schröter, J. Ullrich, R. Moshhammer, and J. Biegert, *Phys. Rev. X* **5**, 021034 (2015).
- [51] M. Kübel, K. J. Betsch, N. G. Kling, A. S. Alnaser, J. Schmidt, U. Kleineberg, Y. Deng, I. Ben-Itzhak, G. G. Paulus, T. Pfeifer, J. Ullrich, R. Moshhammer, M. F. Kling, and B. Bergues, *New. J. Phys.* **16**, 033008 (2014).
- [52] J. Chen, J. Liu, L. B. Fu, and W. M. Zheng, *Phys. Rev. A* **63**, 011404(R) (2000).
- [53] J. Chen, and C. H. Nam, *Phys. Rev. A* **66**, 053415 (2002).
- [54] X. L. Hao, G. Q. Wang, X. Y. Jia, W. D. Li, J. Liu, and J. Chen, *Phys. Rev. A* **80**, 023408 (2009).
- [55] X. L. Hao, W. D. Li, J. Liu, and J. Chen, *Phys. Rev. A* **83**, 053422 (2011).
- [56] B. Hu, J. Liu, and S. G. Chen, *Phys. Lett. A* **236**, 533 (1997).
- [57] N. B. Delone, and V. P. Krainov, *J. Opt. Soc. Am. B* **8**, 1207 (1991).
- [58] L. D. Landau, and E. M. Lifshitz, *Quantum Mechanics* (Pergamon Press, 1977).
- [59] A. N. Pfeiffer, C. Cirelli, M. Smolarski, D. Dimitrovski, M. Abu-samaha, L. B. Madsen and U. Keller, *Nat. Phys.* **8**, 76 (2012).
- [60] J. S. Cohen, *Phys. Rev. A* **26**, 3008 (1982).
- [61] X. Y. Jia, X. L. Hao, D. H. Fan, W. D. Li, and J. Chen, *Phys. Rev. A* **88**, 033402 (2013).
- [62] S. V. Popruzhenko, Ph. A. Korneev, S. P. Goreslavski, and W. Becker, *Phys. Rev. Lett.* **89**, 023001 (2002).
- [63] C. Figueira de Morisson Faria, and W. Becker, *Laser Phys.* **13**, 1196 (2003).
- [64] K. G. Dyall, I. P. Grant, F. A. Parpia, and E. P. Plum-

- mer, *Comput. Phys. Commun.* **55**, 425 (1989).
- [65] C. A. Mancuso, K. M. Dorney, D. D. Hickstein, J. L. Chaloupka, J. L. Ellis, F. J. Dollar, R. Knut, P. Grychtol, D. Zusin, C. Gentry, M. Gopalakrishnan, H. C. Kapteyn, and M. M. Murnane, *Phys. Rev. Lett.* **117**, 133201 (2016).
- [66] C. A. Mancuso, D. D. Hickstein, K. M. Dorney, J. L. Ellis, E. Hasović, R. Knut, P. Grychtol, C. Gentry, M. Gopalakrishnan, D. Zusin, F. J. Dollar, X. M. Tong, D. B. Milošević, W. Becker, H. C. Kapteyn, and M. M. Murnane, *Phys. Rev. A* **93**, 053406 (2016).
- [67] H. Niikura, F. Légaré, R. Hasbani, A. D. Bandrauk, M. Yu. Ivanov, D. M. Villeneuve, and P. B. Corkum, *Nature* **417**, 917 (2002).